Research Article

Received: 10 October 2013 Revised: 2 January 2014 Accepted article published: 15 January 2014 Published online in Wiley Online Library:

(wileyonlinelibrary.com) DOI 10.1002/jctb.4324

# Fenton and photo-Fenton processes for the degradation of atrazine: a kinetic study

**Tamara B. Benzaquén,[a] Miguel A. Isla[a,b] and Orlando M. Alfano[a,b*]**

## Abstract

**BACKGROUND: This study is focused on the kinetic modelling of the Fenton and photo-Fenton degradation of a model pollutant (atrazine) in aqueous solution. The effects of hydrogen peroxide and ferric ion concentrations as well as those of radiation level on the atrazine degradation processes have been investigated.**

**RESULTS: The experimental work was performed in a well-stirred tank laboratory reactor irradiated from both sides with two tubular UV-lamps. The reaction rate expressions were derived from an accepted reaction mechanism, explicitly taking into account the local volumetric rate of photon absorption inside the photoreactor. The proposed kinetic model was able to reproduce the combined effects of changing the ferric iron concentrations, hydrogen peroxide to atrazine molar ratios and radiation level on the pollutant degradation rate. Model predictions were compared with experimental data and good agreement was obtained. The maximum root mean square error (RMSE) for all the estimations was $< 2.5\%$.**

**CONCLUSIONS: The results obtained indicate that Fenton and photo-Fenton processes are possible ways to improve the biodegradability of water containing commercial atrazine.**


**Keywords:** kinetic study; Fenton; photo-Fenton; atrazine; photon absorption

## NOTATION

| | |
|---|---|
| $C$ | molar concentration (mol cm$^{-3}$) |
| $e^a$ | local volumetric rate of photon absorption, LVRPA (einstein cm$^{-3}$ s$^{-1}$) |
| $f$ | normalized spectral distribution of the lamp output power |
| $k$ | kinetic constant (cm$^3$ mol$^{-1}$ s$^{-1}$) |
| $L$ | reactor length (cm) |
| MAE | mean absolute error (%) |
| RMSE | root mean square error (%) |
| R | hydrogen peroxide to atrazine molar ratio (dimensionless) |
| $R$ | reaction rate (mol cm$^{-3}$ s$^{-1}$) |
| $q_w$ | net radiative flux at the reactor wall (einstein cm$^{-2}$ s$^{-1}$). |
| t | time (s). |
| $V$ | volume (cm$^3$) |
| $x$ | spatial coordinate (cm) |
| $X_i$ | coded variable |

*Greek Letters*

| | |
|---|---|
| $\alpha$ | molar absorptivity (cm$^2$ mol$^{-1}$) |
| $\lambda$ | wavelength (nm) |
| $\Phi$ | primary quantum yield (mol einstein$^{-1}$) |

*Subscripts*

| | |
|---|---|
| ATZ | relative to atrazine. |
| $H_2O_2$ | relative to hydrogen peroxide |
| $Fe^{3+}$ | relative to ferric ion |
| $Fe^{2+}$ | relative to ferrous ion |
| i | relative to species (i) |
| R | a reactor property |
| T | a tank property |
| W | a reactor wall property |
| $\lambda$ | indicates a dependence on wavelength |

*Superscripts*

| | |
|---|---|
| 0 | initial condition |
| T | thermal rate |

*Special symbol*

| | |
|---|---|
| $\langle\square\rangle$ | average value |

## INTRODUCTION

Traditional treatment methods such as biological methods are ineffective to degrade some recalcitrant organic pollutants, due to their resistance to biodegradation.[1–3] In recent years, advanced oxidation processes (AOPs), capable of generating highly reactive hydroxyl radicals (•OH), have been investigated by many

* *Correspondence to: O.M. Alfano, INTEC (UNL-CONICET), Ruta Nacional N° 168, 3000 Santa Fe, Argentina. E-mail: alfano@santafe-conicet.gov.ar*

a *INTEC (UNL-CONICET), Ruta Nacional N° 168, 3000 Santa Fe, Argentina*

b *Departamento de Medio Ambiente, FICH, Ciudad Universitaria CC 242 Paraje El Pozo, 3000 Santa Fe, Argentina*

 

researchers due to their ability to oxidize and mineralize a great variety of toxic and non-biodegradable compounds.[4,5]

Among these AOPs, Fenton and photo-Fenton systems are becoming increasingly attractive in treating industrial effluents, because iron is a non-expensive, abundant, and non-toxic substance, and hydrogen peroxide is one of the most versatile, dependable, and environmentally friendly oxidizing agents available. Therefore, these processes appear as effective alternative methods to treat recalcitrant organic pollutants like most agrochemicals.[6,7]

Atrazine [2-chloro-4-(ethylamino)-6-(isopropylamino)-striazine] has been chosen as a model compound in this study because it is still one of the most widely used herbicides worldwide. It is a selective absorbing herbicide which can be used in corn fields, mainly for controlling broadleaf and grassy weeds on both agricultural and non-agricultural land.[8–10] Atrazine was classified as a probable human carcinogen by the USEPA.[11] Most human exposure is originated in the consumption of contaminated water. Furthermore, even low concentrations of this herbicide adversely affect the sexual development of amphibians.[12] This common soil and water pollutant, not readily biodegradable,[7,13,14] presents relatively high persistence in soils (half-life of weeks to months) and even reaches the groundwater.[15]

The object of the present work was to study the degradation of atrazine in aqueous solution using Fenton and photo-Fenton systems. The main purpose of this investigation was first to develop and validate a kinetic model with its kinetic parameters to predict the degradation rates of the involved organic compounds and then to evaluate the effects of the different operating conditions on the behaviour of a photo-Fenton reactor. Thus, a kinetic model derived from a well-known reaction sequence was proposed to predict the concentrations of atrazine, hydrogen peroxide and ferric ion, in a laboratory scale photochemical reactor operated in batch mode. The kinetic parameters were estimated using three ferric iron concentrations and different hydrogen peroxide to atrazine molar ratios (R). Afterwards, predicted and experimental concentrations were compared and analysed as a function of time.

## EXPERIMENTAL

Photodegradation of atrazine was carried out in an isothermal, well-stirred batch recycling reactor. Figure 1 shows a schematic representation of the experimental setup. The flat-plate reactor made of borosilicate (Pyrex) glass and circular cross-section was irradiated from both sides with two tubular black light UV-lamps (TLK40W/09N, Philips) placed at the focal axis of two cylindrical reflectors of parabolic cross-section. The lamps emit radiation in the range 315–400 nm, with a peak at 365 nm.

The complete reacting system was operated in a closed recirculating circuit driven by a high flow rate centrifugal pump and with a well-stirred borosilicate glass reservoir tank, which was equipped with a liquid sampling valve, a thermometer and pH control. The experimental setup had an all-glass heat exchanger connected to a thermostatic bath, to keep the temperature constant during the experimental runs.

The experimental procedure started when the previously prepared atrazine solution ($C_8H_{14}ClN_5$, commercial formulation 90%, SYNGENTA) was incorporated to the storage tank in order to achieve a herbicide concentration of 15 mg $L^{-1}$. A ferric sulphate solution ($FeSO_4.nH_2O$, Carlo Erba, RPE) and distilled water were also incorporated so as to reach the desired

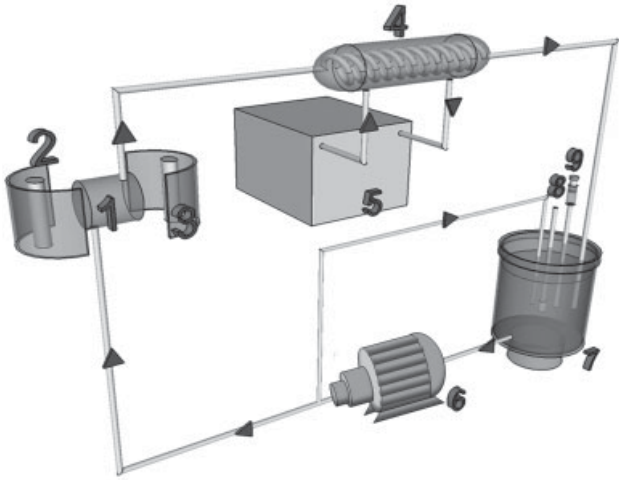


**Figure 1.** Schematic representation of the experimental setup: 1 – photoreactor, 2 – UV lamp, 3 – parabolic reflector, 4 – heat exchanger, 5 – thermostatic bath, 6 – pump, 7 – storage tank, 8 – liquid sampling and 9 – thermometer.

concentration.Then, concentrated sulphuric acid (95–98% Pro-analysis, Ciccarelli p.a.) was added to the mixture to adjust the pH. The pH and temperature were kept constant throughout the experiments at 2.8–3.0 and 298 K, respectively. This is the optimum pH when this iron salt is employed.[16] Afterwards, the hydrogen peroxide solution was added (reagent-grade, 30% w/v, Ciccarelli p.a.) and the reacting mixture was well homogenised by recirculation. The pump flow rate (83.3 $cm^3$ $s^{-1}$) provided good mixing conditions. During this time interval, the reactor glass window was shaded with a shutter located between each lamp and reactor window, to avoid radiation from entering. Then, the first sample was withdrawn and the shutters were immediately removed to start the photo-Fenton experiments (reaction time equal to zero). During the experimental runs, aliquots of the aqueous suspensions were collected at regular times and filtered through 0.45 nylon filters (Millipore) and, as soon as the sample was withdrawn, the Fenton reaction was stopped instantaneously by adding methanol.

A set of experimental runs for Fenton and photo-Fenton reactions was performed, using different values of the hydrogen peroxide to atrazine initial molar ratios and three ferric iron concentrations. For this purpose, an experimental design method was adopted and the effect of the following working variables were investigated: (i) ferric iron concentrations, $C^0_{Fe^{3+}}$ (mg $L^{-1}$) = [5–25]; (ii) hydrogen peroxide to atrazine initial molar ratios, R = [35–350]; and (iii) two irradiation levels, Radiation = [0–1] (corresponding to dark or irradiated solution). These working variables were called $X_1$, $X_2$, and $X_3$, respectively. Table 1 presents a summary of the operating conditions and coded variables for the experimental runs.

### Analysis

Atrazine concentration was measured by HPLC (Waters, Model Code 5CH) using reverse phase liquid chromatography equipped with a UV detector and a C-18 column (X-Terra® RP). The eluent was a binary mixture of distilled water and acetonitrile in proportion 50:50; the eluent flow rate was 1 mL $min^{-1}$ and the detection was performed at 221 nm. Hydrogen peroxide was analysed by means of a modified iodimetric technique using a UV-VIS CARY 100 BIO, at 350 nm[17] and ferrous ions with absorbance measurements of the $Fe^{2+}$-phenantroline complex, at 510 nm.[18]

**Table 1.** Experimental plan and matrix

| Experimental plan | | | Experimental matrix | | |
|---|---|---|---|---|---|
| $C^0_{Fe^{3+}}$ | R | Radiation | $X_1$ | $X_2$ | $X_3$ |
| 5 | 35 | with | −1 | −1 | 1 |
| 5 | 175 | with | −1 | 0 | 1 |
| 5 | 350 | with | −1 | 1 | 1 |
| 15 | 35 | with | 0 | −1 | 1 |
| 15 | 175 | with | 0 | 0 | 1 |
| 15 | 350 | with | 0 | 1 | 1 |
| 25 | 35 | with | 1 | −1 | 1 |
| 25 | 175 | with | 1 | 0 | 1 |
| 25 | 350 | with | 1 | 1 | 1 |
| 5 | 35 | without | −1 | −1 | 0 |
| 5 | 175 | without | −1 | 0 | 0 |
| 5 | 350 | without | −1 | 1 | 0 |
| 15 | 35 | without | 0 | −1 | 0 |
| 15 | 175 | without | 0 | 0 | 0 |
| 15 | 350 | without | 0 | 1 | 0 |
| 25 | 35 | without | 1 | −1 | 0 |
| 25 | 175 | without | 1 | 0 | 0 |
| 25 | 350 | without | 1 | 1 | 0 |

## KINETIC MODEL

A kinetic model for the degradation of atrazine in water solution for the Fenton and photo-Fenton processes was developed. The reaction mechanism used in this paper is based on the reaction scheme reported in detail elsewhere.[16,19–21] The reaction scheme is illustrated in Table 2.

Previous studies have shown that the degradation of atrazine by AOPs leads to the formation of one final product, rather than complete oxidation. This behaviour can be attributed to the strong stability of this product (cyanuric acid, CNA) toward further oxidation during the attack of hydroxyl radicals in the photodegradation.[23–27] However, there is some evidence that cyanuric acid has a lower toxicity than atrazine and is more biodegradable.[28] Thus, it can be removed by biological treatment.[29]

A kinetic model was developed that can account for the reaction rates of atrazine, hydrogen peroxide and ferrous ion. In order to accomplish this, we have considered the following assumptions:

**Table 2.** Reaction scheme for the Fenton and photo-Fenton degradation of atrazine

| Number | Reaction step | Constant |
|---|---|---|
| 0 | $Fe^{3+} + H_2O \rightarrow Fe^{2+} + {}^{\bullet}OH + H^+$ | $\Phi_{Fe^{2+},\lambda}$ |
| 1 | $Fe^{3+} + H_2O_2 \rightarrow Fe^{2+} + H^+ + HO^{\bullet}{}_2$ | $k_1$ |
| 2 | $Fe^{2+} + H_2O_2 \rightarrow Fe^{3+} + OH^- + {}^{\bullet}OH$ | $k_2$ |
| 3 | $H_2O_2 + {}^{\bullet}OH \rightarrow HO^{\bullet}{}_2 + H_2O$ | $k_3$ |
| 4 | $Fe^{2+} + {}^{\bullet}OH \rightarrow Fe^{3+} + OH^-$ | $k_4$ |
| 5 | $H_2O_2 + HO^{\bullet}{}_2 \rightarrow {}^{\bullet}OH + H_2O + O_2$ | $k_5$ |
| 6 | $2{}^{\bullet}OH \rightarrow H_2O_2$ | $k_6$ |
| 7 | $2HO^{\bullet}{}_2 \rightarrow H_2O_2 + O_2$ | $k_7$ |
| 8 | $HO^{\bullet}{}_2 + {}^{\bullet}OH \rightarrow H_2O + O_2$ | $k_8$ |
| 9 | $Fe^{3+} + HO^{\bullet}{}_2 \rightarrow Fe^{2+} + H^+ + O_2$ | $k_9$ |
| 10 | $Fe^{2+} + HO^{\bullet}{}_2 + H^+ \rightarrow Fe^{3+} + H_2O_2$ | $k_{10}$ |
| 11 | $ATZ + {}^{\bullet}OH \rightarrow Products + Cl^- + NO_3{}^-$ | $k_{11}$ |

(i) the steady-state approximation (SSA) may be applied for highly reactive intermediates, (such as $^{\bullet}OH$ and $HO_2{}^{\bullet}$ radicals),
(ii) radical–radical termination reactions are neglected compared with the propagation reactions,
(iii) the oxygen concentration is always in excess,
(iv) reaction step 5 is neglected.[22]

With these assumptions, the following reaction rates can be derived (see Appendix):

$$\begin{bmatrix} R_{ATZ}(x,t) \\ R_{H_2O_2}(x,t) \\ R_{Fe^{2+}}(x,t) \end{bmatrix} = \begin{bmatrix} R^T_{ATZ}(t) \\ R^T_{H_2O_2}(t) \\ R^T_{Fe^{2+}}(t) \end{bmatrix} + \Phi_{Fe^{2+},\lambda} \sum_{\lambda} e^a_{\lambda}(x,t) \begin{bmatrix} -\frac{1}{\alpha} \\ -\left(\frac{\alpha'}{\alpha\beta}\right) \\ \left(\frac{1}{\alpha}\right)\left(\frac{2\alpha'}{\beta}+1\right) \end{bmatrix} \quad (1)$$

where

$$\begin{bmatrix} R^T_{ATZ}(t) \\ R^T_{H_2O_2}(t) \\ R^T_{Fe^{2+}}(t) \end{bmatrix} = k_1 C_{H_2O_2} C_{Fe^{3+}} \begin{bmatrix} 0 \\ -\frac{1}{\beta} \\ \frac{2}{\beta} \end{bmatrix} + k_2 C_{H_2O_2} C_{Fe^{2+}} \begin{bmatrix} -\frac{1}{\alpha} \\ -\left(1+\frac{\alpha'}{\alpha\beta}\right) \\ \left(\frac{1}{\alpha}\right)\left(\frac{2\alpha'}{\beta}-2\alpha+1\right) \end{bmatrix} \quad (2)$$

Here, the following kinetic parameters have been defined:

$$\alpha = \frac{k_3 C_{H_2O_2}}{k_{11} C_{ATZ}} + \frac{k_4 C_{Fe^{2+}}}{k_{11} C_{ATZ}} + 1 \quad (3)$$

and

$$\beta = \frac{k_{10} C_{Fe^{2+}}}{k_9 C_{Fe^{3+}}} + 1 \quad (4)$$

where $R_i(x,t)$ (with $i = ATZ, H_2O_2, Fe^{+2}$) are the local reaction rates, $C_{ATZ}$, $C_{H_2O_2}$, $C_{Fe^{3+}}$ and $C_{Fe^{2+}}$ are the atrazine, hydrogen peroxide, ferric ion and ferrous ion concentrations, respectively; $k_i$ are the kinetic constants defined in the reaction scheme (Table 2); $\Phi$ is the wavelength-averaged primary quantum yield, and $e^a_{\lambda}$ is the spectral local volumetric rate of photon absorption (LVRPA).

In Equation (1), the first term on the right-hand side symbolizes the thermal reaction rate (Fenton system) and the second term on the right-hand side corresponds to the photochemical reaction rate (photo-Fenton reaction).

## REACTOR MODEL

### Mass balances

The experimental device employed for the Fenton and photo-Fenton degradation of atrazine was an isothermal, well-stirred batch recycling reactor. For the kinetic studies, the mass balances and the initial conditions for the atrazine, hydrogen peroxide and ferrous iron are given by the following mathematical expressions:[30]

$$\frac{dC_i(t)}{dt} = \frac{V_R}{V}\langle R_i(x,t)\rangle_{V_R} + \frac{(V-V_R)}{V} R^T_i(t), \quad (i = ATZ, H_2O_2 \text{ and } Fe^{2+}) \quad (5)$$

with the initial conditions

$$C_i\left(t_0\right) = C_i^0, \qquad \left(i = ATZ, H_2O_2 \text{ and } Fe^{2+}\right) \tag{6}$$

where $R_i$ and $R_i^T$ are the photo-Fenton and Fenton reactions, respectively. Again, note that the first term on the right-hand side of Equation (5) represents the organic pollutant degradation produced by both the light-activated and thermal reactions (photo-Fenton) that take place in the irradiated liquid volume ($V_R$), and the second term on the right-hand side corresponds to the contaminant decomposition generated by the thermal or dark reaction (Fenton) occurring in the non-irradiated volume ($V - V_R$).

The required reaction rates for the mass balances can be obtained from the kinetic model given by Equations (1–4).

### Volumetric rate of photon absorption

For the numerical evaluation of the mass balances, it is necessary to introduce the LVRPA averaged over the reactor volume on the right-hand side of Equation (5). In this case, a flat-plate reactor of a circular cross-section was irradiated from both sides with two tubular lamps placed at the focal axis of two parabolic reflectors; consequently, similar expressions may be used for each emitting system. Figure 2 shows more details of the system: photoreactor – radiation sources – reflectors.

In a previous work, a radiation model was developed to evaluate the spectral LVRPA averaged over the reactor volume for this emitting system.[27] In agreement with the representation proposed by Rossetti *et al.*, a one-dimensional (1-D) radiation field model was used to calculate the monochromatic LVRPA as a function of the spatial coordinate (x) and time (t). It was also considered that the iron complex $Fe(OH)^{2+}$ was the dominant species at pH = 3.[31] Besides, radiation absorption of ferrous ion ($Fe^{2+}$) and hydrogen peroxide ($H_2O_2$) was negligible for a wavelength $\lambda > 300$ nm. Thus, the LVRPA averaged over the reactor volume can be evaluated by:

$$\left\langle \sum_\lambda e_\lambda^a\left(x,t\right)\right\rangle_{V_R} = \sum_\lambda \frac{2\, q_W f_\lambda}{L}\left[1 - \exp\left(-\alpha_{Fe(OH)^{2+},\lambda} C_{Fe(OH)^{2+}}\left(t\right) L\right)\right] \tag{7}$$

where, $x$ is the spatial coordinate, $t$ the reaction time, $q_W$ is the net radiative flux at the reactor wall, $f_\lambda$ is the normalized spectral distribution of the lamp output power provided by the lamp manufacturer, and $\alpha_{Fe(OH)^{2+}}$ is the molar absorptivity and $C_{Fe(OH)^{2+}}$ the molar concentration of the light absorbing species $[Fe(OH)^{2+}]$.

**Table 3.** Estimated values of kinetic parameters with confidence interval (95%)

| Parameters | Values | Confidence interval (95 %) | Units |
|---|---|---|---|
| $k_2$ | $1.530 \times 10^3$ | $\pm 0.056 \times 10^3$ | $M^{-1}\ s^{-1}$ |
| $k_3$ | $7.777 \times 10^8$ | $\pm 0.047 \times 10^8$ | $M^{-1}\ s^{-1}$ |
| $k_{11}$ | $3.281 \times 10^{11}$ | $\pm 0.015 \times 10^{11}$ | $M^{-1}\ s^{-1}$ |

**Table 4.** Root mean square error (RMSE) and mean absolute error (MAE)

| | | Fenton | | Photo-Fenton | |
|---|---|---|---|---|---|
| | Weight factor | RMSE % | MAE % | RMSE % | MAE % |
| ATZ | 0. 40 | 2.17 | 1.57 | 2.79 | 1.68 |
| $H_2O_2$ | 0.60 | 1.97 | 1.54 | 2.23 | 1.74 |
| $ATZ + H_2O_2$ | 1.00 | 2.07 | 1.55 | 2.53 | 1.71 |

## RESULTS AND DISCUSSION

### Parameters estimation

A non-linear least-squares regression procedure based on the Levenberg–Marquardt optimization algorithm was applied to estimate the kinetic parameters. This procedure was employed to provide the values of parameters that minimize the sum of squared differences between predicted concentrations and experimental data of the atrazine and hydrogen peroxide concentrations. To obtain the theoretical concentrations, the system of three nonlinear, first-order, ordinary differential equations (Equations (5) and (6)) was solved numerically using a fourth-order, Runge–Kutta method.

For the numerical solution, it was necessary to obtain the following information:

(i) The values of the kinetic constants were obtained from Walling and Goosen [18] and Buxton *et al.*[32]
(ii) The potassium ferrioxalate actinometry was used to evaluate the radiative flux at the reactor wall. From these experiments, it was determined that $q_W$ is equal to $4.32 \times 10^{-9}$ Einstein $cm^{-2}\ s^{-1}$.
(iii) The molar absorptivity of the absorbing species $[Fe(OH)^{2+}]$ was obtained from the specific literature.[31]
(iv) The wavelength-averaged primary quantum yield ($\Phi_{Fe^{2+},\lambda}$) was taken from Farias *et al.*[33]

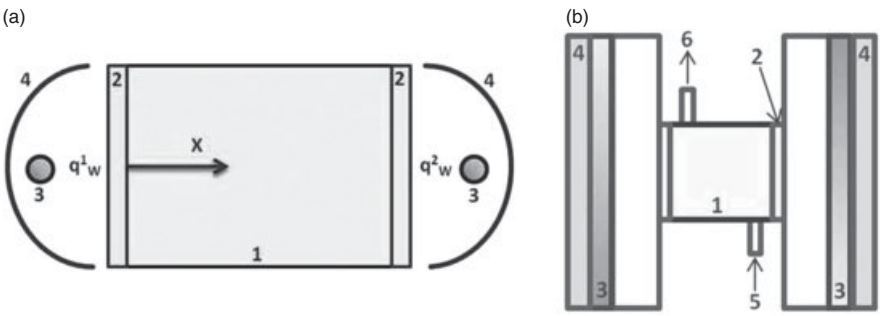


**Figure 2.** Schematic representation of the system: photoreactor – radiation sources – reflectors. 1 – Reactor, 2 – Glass windows, 3 – Lamps, 4 – Reflectors, 5 – inlet and 6 – outlet: (a) top view and (b) side view.

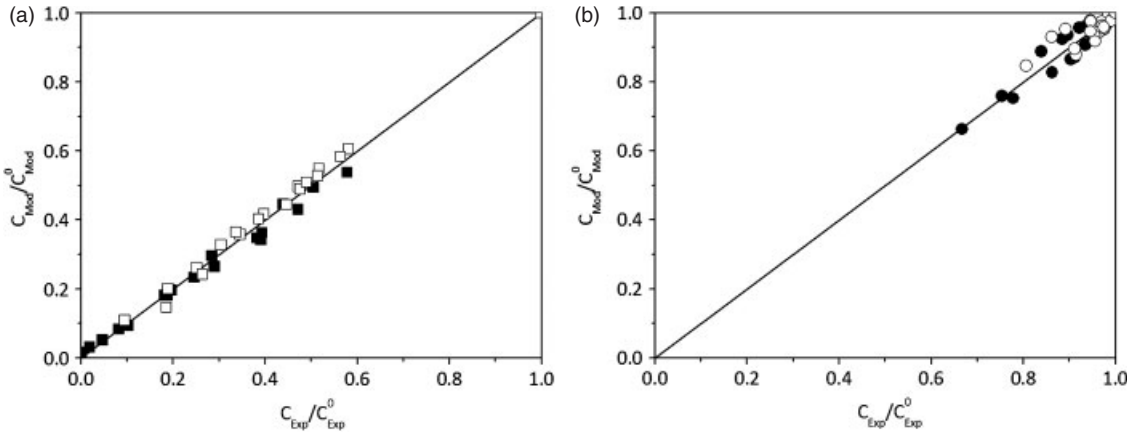


**Figure 3.** Experimental vs. predicted concentrations. (a) Atrazine (□, ■) and (b) hydrogen peroxide (○, ●). Fenton (□, ○) and photo-Fenton (■, ●).

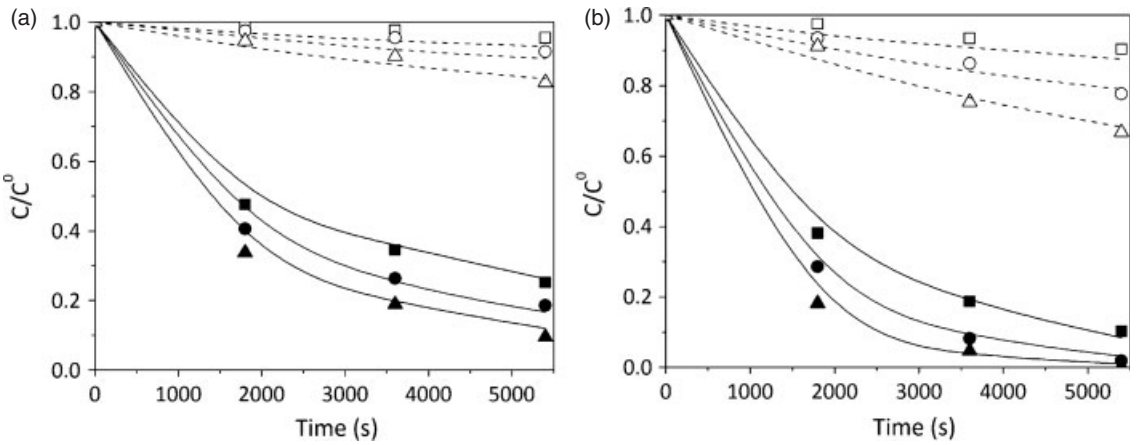


**Figure 4.** Experimental vs. predicted relative concentrations. (a) Fenton and (b) photo-Fenton reactions. R = 350, with $C^0_{Fe^{3+}}$ = 5 ppm (■, □), 15 ppm (●, ○) and 25 ppm (▲, △). Hydrogen peroxide (_ _ _) and atrazine (____).

It should also be noted that the ferric ion concentration as a function of time may be determined from the initial ferric ion concentration ($C^0_{Fe^{3+}}$) and the actual ferrous ion concentration ($C_{Fe^{2+}}$).

By using the atrazine and hydrogen peroxide experimental concentrations versus time data and the nonlinear regression algorithm mentioned above, three parameters were adjusters: $k_2$, $k_3$ and $k_{11}$. These three kinetic constants were chosen due to the high sensitivity of the kinetic model to their values. Besides, in order to further improve the predictions of the pollutant degradation, a weight factor (F) was determined to compute the objective function and reach the minimum value of the root mean square error (RMSE).

Estimated values of the kinetic parameters are presented in Table 3. It should be noted that the result obtained for $k_{11}$ is reasonable, according to the range of values reported in the literature. [34] It is worth noting that the estimated values for $k_2$ and $k_3$ did not differ significantly from those reported for Walling and Goosen.[18]

A root mean square error (RMSE) and a mean absolute error (MAE) were used to evaluate the accuracy of the model. Results are summarized in Table 4. It has to be stressed that the experimental data set used in this kinetic model study had a total of 144 points.

Figure 3 shows predicted and experimental concentrations for all the Fenton and photo-Fenton runs performed in the kinetic study. The symbols correspond to the atrazine and hydrogen peroxide concentrations obtained at different reaction times, for all the experimental runs performed in this photoreactor.

Model predictions were compared with experimental data and a good agreement was obtained, with a RMSE of 2.07% for the Fenton system and 2.53% for the photo-Fenton system (Table 4). For all the investigated Fenton and photo-Fenton experimental runs, and considering atrazine and hydrogen peroxide concentrations, the RMSE of the estimations was 2.31%.

## Atrazine degradation

The effects of $C^0_{Fe^{3+}}$ and R on the atrazine degradation for the Fenton and photo-Fenton reactions were analysed. The influence of the initial iron concentration on the relative atrazine and hydrogen peroxide concentrations, for a constant value of R, is presented in Fig. 4. Typical data presented in this figure show that the relative concentrations of atrazine and hydrogen peroxide were adequately predicted by the kinetic model.

Looking at the atrazine concentrations in the figures, it should be noted that an increase of the initial iron concentration from 5 to 25 ppm introduces an increase on the pollutant conversion.

The regeneration of ferrous iron from ferric iron is the rate limiting step in the catalytic iron cycle, if iron is added in small amounts.[35] Previous studies have also found that an increase in iron concentration always leads to an increased reaction rate.[36–39]

  

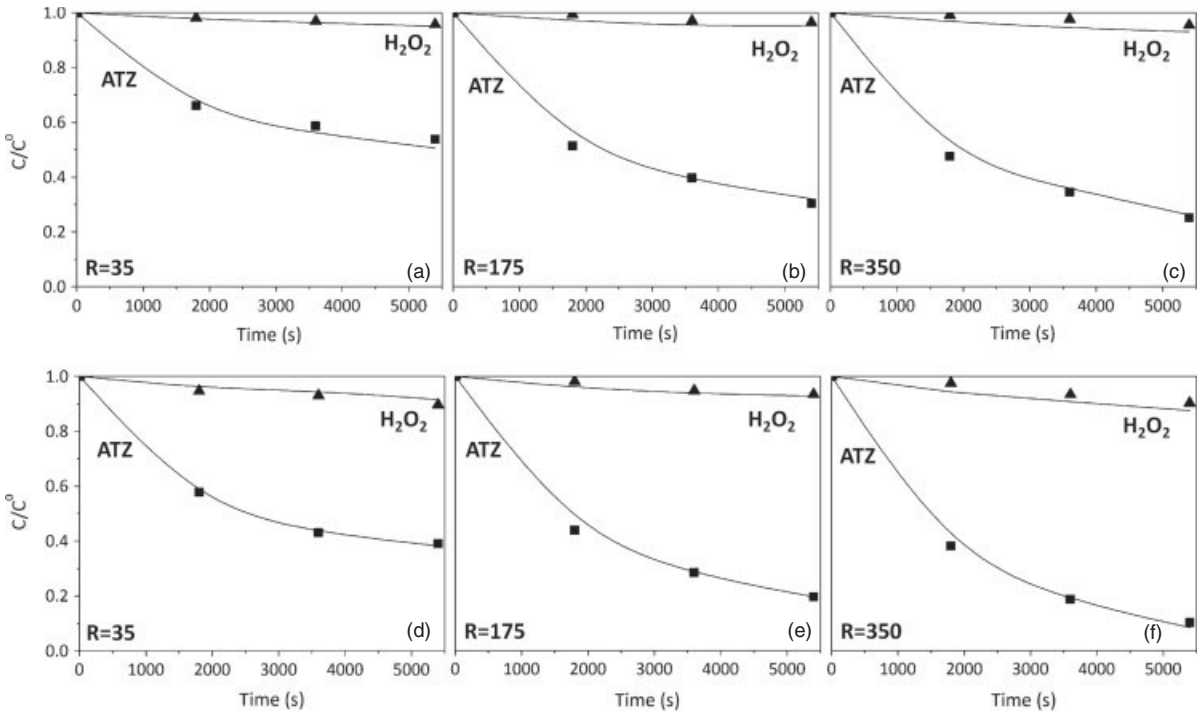


**Figure 5.** Experimental and predicted relative concentrations of atrazine and hydrogen peroxide vs. time for $C^0_{Fe^{3+}} = 5$ ppm. Fenton reaction: (a) R = 35, (b) R = 175 and (c) R = 350; and photo-Fenton reaction: (d) R = 35, (e) R = 175 and (f) R = 350. Experimental data: atrazine (■) and hydrogen peroxide (▲). Model results: solid lines.

To investigate the effects of the initial hydrogen peroxide concentration on the atrazine degradation, different hydrogen peroxide to atrazine initial molar ratios (*R*) were compared using constant values of the $C^0_{Fe^{3+}}$. The experiments were carried out changing *R* from 35 to 350. The atrazine and hydrogen peroxide relative concentrations by Fenton and photo-Fenton treatment as a function of time are shown in Fig. 5.

These results show that an increase of the hydrogen peroxide to atrazine molar ratio introduces an important atrazine conversion enhancement. Accordingly, knowing that the reaction rate generating hydroxyl radicals generally increases with increase of hydrogen peroxide concentration, it was reasonable to expect that pollutant degradation was strongly dependent on an increase in hydrogen peroxide concentration.[40] However, it should be taken into account that an extremely high concentration of hydrogen peroxide may generate some unwanted side reactions that consume valuable hydroxyl radicals in the solution (Table 3, reaction steps 3 and 5).[19]

In general, higher iron or hydrogen peroxide concentrations result in faster decay rate and higher oxidation capacity. However, it should be noted that the increase of the atrazine degradation obtained by increasing R is higher than the slight increase of the pollutant degradation rate obtained by increasing the iron concentration.

The most effective $C^0_{Fe^{3+}}$ and R values for degradation of atrazine by both Fenton and photo-Fenton treatments were 25 mg $L^{-1}$ and 350, respectively. However, it is interesting to note that the results obtained with R = 350 and $C^0_{Fe^{3+}} = 25$ ppm for the Fenton reaction do not differ significantly from those obtained with R = 175 and $C^0_{Fe^{3+}} = 15$ ppm for the photo–Fenton reaction, as seen in Fig. 6.

Finally, Fig. 7 shows the effects of irradiation on the relative atrazine and hydrogen peroxide concentrations. Comparing the Fenton and photo-Fenton herbicide degradation, one can notice

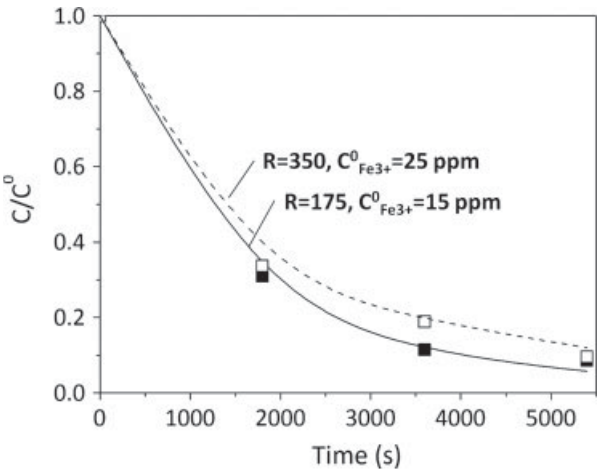


**Figure 6.** Experimental vs. predicted relative concentrations of atrazine for R = 175 and $C^0_{Fe^{3+}} = 15$ ppm (■), and for R = 350 and $C^0_{Fe^{3+}} = 25$ ppm (□). Fenton (_ _ _) and (b) photo-Fenton (___).

that for a constant value of R and $C^0_{Fe^{3+}}$, the photo–Fenton conversion is always higher than that obtained with the Fenton system.

It is known that in the photo-Fenton reaction the UV-Visible irradiation contributes to the formation of •OH radicals by photolysis of $Fe^{3+}$ complex ions, as shown by the first reaction step of Table 2; thus, the chemical oxidation is accelerated by radiation. However, under certain experimental conditions of $C^0_{Fe^{3+}}$ and ratio $C^0_{H_2O_2}/C^0_{ATZ}$, the herbicide conversion for the photo-Fenton reaction is not considerably higher than that obtained with the non-irradiated system. It was demonstrated that both the photo-Fenton reaction using iron and hydrogen peroxide at low

  

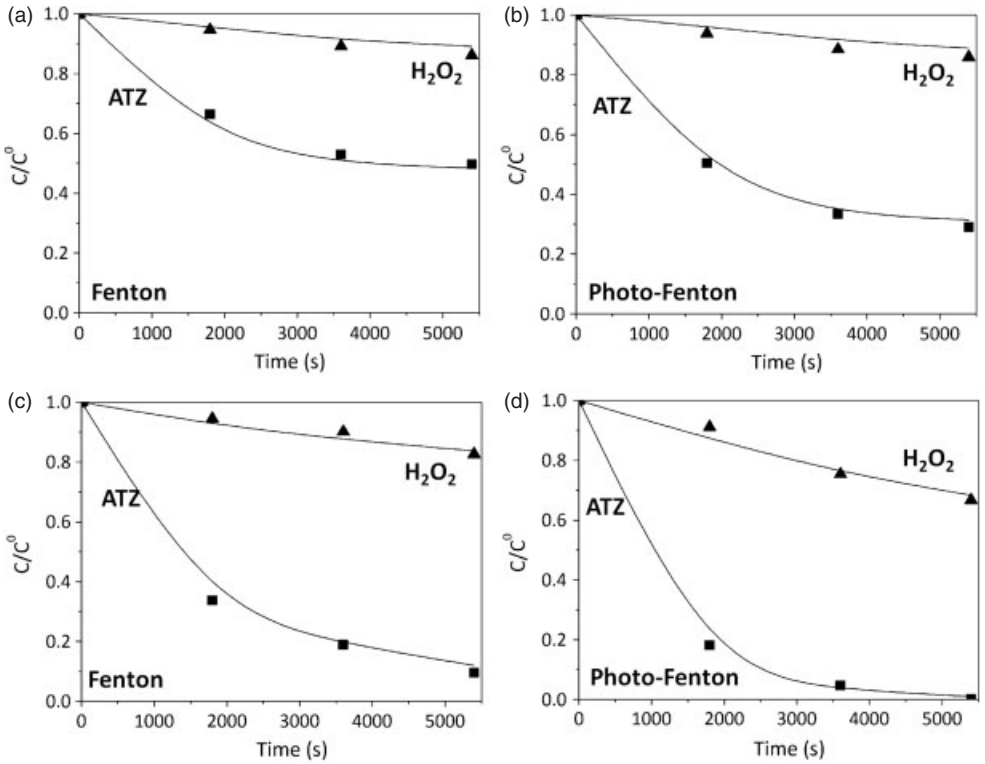


**Figure 7.** Experimental and predicted concentrations of atrazine and hydrogen peroxide vs. time for $C^0_{Fe^{3+}} = 25$ ppm. (a) Fenton reaction, R = 35; (b) photo-Fenton reaction, R = 35; (c) Fenton reaction, R = 350; and (d) photo-Fenton reaction, R = 350. Experimental data: atrazine (■) and hydrogen peroxide (▲). Model results: solid lines.

concentrations and the Fenton reaction with iron and hydrogen peroxide at high concentrations are feasible treatments for water containing a moderately low concentration of atrazine. As explained before, the degradation of atrazine by the photo-Fenton reaction leads to the formation of cyanuric acid as final product. However, it was verified that cyanuric acid has a lower toxicity than atrazine and is more biodegradable.[41,42] Consequently, the partial mineralization of atrazine employing a photo-Fenton process, followed by a biological treatment to degrade cyanuric acid, is a feasible treatment option for the complete mineralization of atrazine contaminated wastewater.

## CONCLUSIONS

A kinetic model to represent the Fenton and photo-Fenton oxidation of atrazine in a well-stirred batch recycling reactor was developed. First, the kinetic model was proposed and validated with its kinetic parameters to predict the degradation rates of the involved organic compounds. Then the effects of the different operating conditions on the behaviour of a laboratory photo-Fenton reactor were evaluated.

When predictions of the kinetic model were compared with experimental data, a good representation of the atrazine and hydrogen peroxide concentrations as a function of time was obtained. This comparison was performed for different ferric iron concentrations, hydrogen peroxide to atrazine initial molar ratios and radiation levels. The root mean square errors for the Fenton and photo-Fenton systems were 2.07% and 2.53%, respectively. Considering both atrazine and hydrogen peroxide concentrations for Fenton and photo-Fenton experimental runs, the maximum RMSE of the estimations was 2.31%.

It was demonstrated that both photo-Fenton reaction employing iron and hydrogen peroxide at low concentrations and Fenton reaction using iron and hydrogen peroxide at high concentrations are appropriate treatments for water containing atrazine. Consequently, Fenton and photo-Fenton processes are promising pre-treatments capable of enhancing the biodegradability of water contaminated with biorecalcitrant chemicals (atrazine).

## ACKNOWLEDGEMENTS

The authors are grateful to Universidad Nacional del Litoral (UNL), Consejo Nacional de Investigaciones Científicas y Técnicas (CONICET) and Agencia Nacional de Promoción Científica y Tecnológica (ANPCyT). They also thank Antonio C Negro for his valuable help during the experimental work.

## REFERENCES

1 Konstantinou IK and Albanis TA, $TiO_2$-assisted photocatalytic degradation of azo dyes in aqueous solution: kinetic and mechanistic investigations - a review. *Appl Catal B - Environ* **49**:1–14 (2004).
2 Bacardit J, García-Molina V, Bayarri B, Giménez J, Chamarro E, Sans C and Esplugas S, Coupled photochemical-biological system to treat biorecalcitrant wastewater. *Water Sci Technol* **55**:95–100 (2007).
3 Chen CY, Wu PS and Chung YC, Coupled biological and photo-Fenton pretreatment system for the removal of di-(2-ethylhexyl) phthalate (DEHP) from water. *Bioresource Technol* **100**:4531–4534 (2009).
4 Legrini O, Oliveros E and Braun AM, Photochemical process for water treatment. *Chem Rev* **93**:671–698 (1993).
5 Lapertot M, Ebrahimi S, Dazio S, Rubinelli A and Pulgarin C, Photo-Fenton and biological integrated process for degradation of a mixture of pesticides. *J Photochem Photobiol A: Chem* **186**:34–40 (2007).

  

6 Oller I, Malata S, Sanchez-Peréz JA, Maldonado MI and Gassó R, Detoxification of wastewater containing five common pesticides by solar AOPs-biological coupled system. *Catal Today* **129**:69–78 (2007).
7 Benzaquén TB, Benzzo MT, Isla MA and Alfano OM, Impact of some herbicides on the biomass activity in biological treatment plants and biodegradability enhancement by a photo-Fenton process. *Water Sci Technol* **67**:210–216 (2013).
8 Martin-Neto L, Crestana S, Sposito G, Traghetta DG and Vaz CMP, On the interaction mechanisms of atrazine and hydroxyatrazine with humic substances. *Environ Quart* **30**:520–525 (2001).
9 Chan KH and Chu W, Model applications and mechanism study on the degradation of atrazine by Fenton's system. *J Hazard Mater B* **118**:227–237 (2005).
10 Fan, WQ, Yanase T, Morinaga H, Ondo S, Okabe T, Nomura M, Komatsu T, Morohashi KI, Hayes TB, Takayanagi R and Nawata H, Atrazine-induced aromatase expression is SF-1-dependent: implications for endocrine disruption in wildlife and reproductive cancers in humans. *Environ Health Persp* **115**:720–727 (2007).
11 Belluck, DA, Benjamin SL and Dawson T, Groundwater contamination by atrazine and its metabolites: risk assessment, policy and legal implication. In *Pesticide Transformation Products*. American Chemical Society, Washington, DC, 254–273 (1991).
12 Tavera-Mendoza L, Ruby S, Brousseau P, Fournier M, Cyr D and Marcogliese D, Response of the amphibian tadpole Xenopus laevis to atrazine during sexual differentiation of the ovary. *Environ Toxicol Chem* **21**:1264–1267 (2002).
13 Readman JW, Albanis TA, Barcelo D, Galassi S, Tronczynski J and Gobrielides GP, Herbicide contamination of Mediterranean estuarine waters: results from a MED POL pilot survey. *Marine Pollut Bull* **26**:613–619 (1993).
14 Scott JP and Ollis DF, Integration of chemical and biological oxidation processes for water treatment: review and recommendations. *Environ Progress* **14**:88–103 (1995).
15 Erickson L and Lee KH, Degradation of Atrazine and related s-Triazines. *CRC Cr Rev Env Contr* **19**:1–14 (1989).
16 Pignatello JJ, Oliveros E and MacKay A, Advanced oxidation processes for organic contaminant destruction based on the Fenton reaction and related chemistry. *Crit Rev Environ Sci Technol* **36**:1 (2006).
17 Allen A, Hochanadel C, Ghormley J and Davis J, Decomposition of water and aqueous solutions under mixed fast neutron and gamma radiation. *J Phys Chem - US* **56**:587–594 (1952).
18 APHA, AWWA, WEF, *Standard Methods for the Examination of Water and Wastewater*, 19th edn. APHA, Washington, 3–68 (1995).
19 Walling C and Goosen A, Mechanism of the ferric ion catalyzed decomposition of hydrogen peroxide. Effect of organic substrates. *J Am Chem S* **95**:2987–2991 (1973).
20 De Laat J and Gallard H, Catalytic decomposition of hydrogen peroxide by Fe(III) in homogeneous aqueous solution: mechanism and kinetic modeling. *Environ Sci Technol* **33**:2726–2732 (1999).
21 De Laat J, Gallard H, Ancelin S and Legube B, Comparative study of the oxidation of atrazine and acetone by $H_20_2$ /UV, FeOII)/UV, Fe(III)/$H_20_2$ /UV and Fe(II) or Fe(III)/$H_20_2$. *Chemosphere* **39**:2693–2706 (1999).
22 Gallard H and De Laat J, Kinetic modelling of Fe(III) / $H_2O_2$ oxidation reactions in dilute aqueous solution using atrazine as a model organic compound. *Water Res* **34**:3107 (2000).
23 Pelizzetti E, Maurino V, Minero C, Carlin V, Pramauro E, Zerbinati O and Tosato ML, Photocatalytic degradation of atrazine and other s-triazine herbicides. *Environ Sci Technol* **24**:1559–1565 (1990).
24 Hincapié M, Maldonado MI, Oller I, Gernjak W, Sánchez-Pérez JA, Ballesteros M and Malato S, Solar photocatalytic degradation and detoxification of EU priority substances. *Catal Today* **101**:203–210 (2005).
25 Hincapié M, Peñuela G, Maldonado M, Malato O, Fernández-Ibáñez P, Oller I, Gernjak W and Malato S, Degradation of pesticides in water using solar advanced oxidation processes. *Appl Catal B - Environ* **64**:272–281 (2006).
26 Maldonado MI, Passarinho PC, Oller I, Gernjak W, Fernández P, Blanco J and Malato S, Photocatalytic degradation of EU priority substances: a comparison between TiO2 and Fenton plus photo-Fenton in a solar pilot plant. *J Photochem Photobiol A: Chem* **185**:354–363 (2007).
27 Benzaquén TB, Isla MA and Alfano OM, Quantum efficiencies of the photo-Fenton degradation of atrazine in water. *Water Sci Technol* **66**:2209–2216 (2012).
28 Lapertot M, Pulgarin C, Fernandez-Ibañez P, Maldonado MI, Pérez-Estradab L, Oller I, Gernjakb W and Malato S, Enhancing biodegradability of priority sustances (pesticides) by solar photo Fenton. *Water Res* **40**:1086–1094 (2006).
29 Chan CY, Tao S, Dawson R and Wong PK, Treatment of atrazine by integrating photocatalytic and biological processes. *Environ Pollut* **131**:45–54 (2004).
30 Rossetti GH, Albizzati ED and Alfano OM, Decomposition of formic acid in a water solution employing the photo-Fenton reaction. *Ind Eng Chem Res* **41**:1436–1444 (2002).
31 Faust BC and Hoigne J, Photolysis of Fe(III)-hydroxy complexes as sources of OH radicals in clouds, fog and rain. *Atmos Environ* **24A**:79–89 (1990).
32 Buxton GV, Greenstock CL, Helman WP and Ross AB, Critical review of rate constants for reactions of hydrated electrons, hydrogen atoms and hydroxylradicals (-OH/-O) in aqueous solution. *J Phys Chem* **17**:513–882 (1988).
33 Farias J, Albizzati ED and Alfano OM, New pilot-plant photo-Fenton solar reactor for water decontamination. *Ind Eng Chem Res* **49**:1265–1273 (2010).
34 Huang CP, Dong C and Tang Z, Advanced chemical oxidation: its present role and potential future in hazardous waste treatment. *J Waste Manage* **13**:361–377 (1993).
35 Malato S, Fernandez-Ibanez P, Maldonado MI, Blanco J and Gernjak W, Decontamination and disinfection of water by solar photocatalysis: recent overview and trends. *Catal Today* **147**:1–59 (2009).
36 Krutzler T, Fallmann H, Maletzky P, Bauer R, Malato S and Blanco J, Solar driven degradation of 4-chlorophenol. *Catal Today* **54**:321–327 (1999).
37 Sarria V, Kenfack S, Guillod O and Pulgarin C, An innovative coupled solar-biological system at field pilot scale for the treatment of biorecalcitrant pollutants. *J Photochem Photobiol A: Chem* **159**:89–99 (2003).
38 Gernjak W, Krutzler T, Glaser A, Malato S, Cáceres J, Bauer R and Fernández-Alba AR, Photo-Fenton treatment of water containing natural phenolic pollutants. *Chemosphere* **50**:71–78 (2003).
39 Gernjak W, Fuerhacker M, Fernández-Ibañez P, Blanco J and Malato S, Solar photo-Fenton treatment – process parameters and process control. *Appl Catal B: Environ* **64**:121–130 (2006).
40 Chu W, Chan KH, Kwan CY and Choi KY, Degradation of atrazine by modified stepwise-Fenton's processes. *Chemosphere* **67**:755–761 (2007).
41 Hu C, Yu JC, Hao Z and Wong PK, Photocatalytic degradation of triazine-containing azo dyes in aqueous TiO2 suspensions. *Appl Catal B: Environ* **42**:47–55 (2003).
42 Fragoeiro S and Magan N, Enzymatic activity, osmotic stress and degradation of pesticide mixtures in soil extract liquid broth inoculated with *Phanerochaete crysosporium* and *Trametes versicolor*. *Environ Microbiol* **7**:348–355 (2005).


## APPENDIX

Considering the assumptions proposed for the kinetic model, the reaction rates for the reacting species *i*, may be represented by the following expressions:

$$R_{ATZ}(x,t) = -k_{11}C_{ATZ}\ C_{.OH} \tag{A.1}$$

$$R_{H_2O_2}(x,t) = -k_1 C_{H_2O_2} C_{Fe^{3+}} - k_2 C_{H_2O_2} C_{Fe^{2+}} - k_3 C_{H_2O_2} C_{.OH} + k_{10} C_{Fe^{2+}} C_{HO_2}. \tag{A.2}$$

$$R_{Fe^{2+}}(x,t) = \Phi_{Fe^{2+},\lambda} \sum_{\lambda} e^{a}_{\lambda}(x,t) + k_1 C_{H_2O_2} C_{Fe^{3+}} - k_2 C_{H_2O_2} C_{Fe^{2+}} - k_4 C_{Fe^{2+}} C_{.OH} + k_9 C_{Fe^{3+}} C_{HO_2}. - k_{10} C_{Fe^{2+}} C_{HO_2}. \tag{A.3}$$

$$R_{Fe^{3+}}(x,t) = -R_{Fe^{2+}}(x,t) \tag{A.4}$$

$$R_{OH\cdot}(x,t) = \Phi_{Fe^{2+},\lambda}\sum_{\lambda} e^{a}_{\lambda}(x,t) + k_2 C_{H_2O_2} C_{Fe^{2+}} - k_3 C_{H_2O_2} C_{\cdot OH} - k_4\, C_{Fe^{2+}} C_{\cdot OH} - k_{11} C_{ATZ}\, C_{\cdot OH} \quad (A.5)$$

$$R_{HO_2^{\cdot}}(x,t) = k_1 C_{H_2O_2} C_{Fe^{3+}} + k_3 C_{H_2O_2} C_{\cdot OH} - k_9 C_{Fe^{3+}} C_{HO_2^{\cdot}} - k_{10} C_{Fe^{2+}} C_{HO_2^{\cdot}} \quad (A.6)$$

Equations (A.1) to (A.6) are solved to obtain the mathematical expressions of $R_i(x,t)$. To do this, the steady state approximation (SSA) may be applied for highly reactive radicals and species with very low concentrations (Equation(A.5) and (A.6)),

$$\Phi_{Fe^{2+},\lambda}\sum_{\lambda} e^{a}_{\lambda}(x,t) + k_2 C_{H_2O_2} C_{Fe^{2+}} = \left(k_3 C_{H_2O_2} + k_4 C_{Fe^{2+}} + k_{11} C_{ATZ}\right) C_{\cdot OH} \quad (A.7)$$

$$k_1 C_{H_2O_2} C_{Fe^{3+}} + k_3 C_{H_2O_2} C_{\cdot OH} = \left(k_9 C_{Fe^{3+}} + k_{10} C_{Fe^{2+}}\right) C_{HO_2^{\cdot}} \quad (A.8)$$

Thus,

$$C_{\cdot OH} = \frac{\Phi_{Fe^{2+},\lambda}\sum_{\lambda} e^{a}_{\lambda}(x,t) + k_2 C_{H_2O_2} C_{Fe^{2+}}}{k_{11} C_{ATZ}\,\alpha} \quad (A.9)$$

$$C_{HO_2^{\cdot}} = \frac{k_1 C_{H_2O_2} C_{Fe^{3+}} + k_3 C_{H_2O_2} C_{\cdot OH}}{k_9 C_{Fe^{3+}}\beta} \quad (A.10)$$

where,

$$\alpha = \frac{k_3 C_{H_2O_2}}{k_{11} C_{ATZ}} + \frac{k_4 C_{Fe^{2+}}}{k_{11} C_{ATZ}} + 1 \text{ and } \beta = \frac{k_{10} C_{Fe^{2+}}}{k_9 C_{Fe^{3+}}} + 1 \quad (A.11)$$

Then, placing Equations (A.9) and (A.10) into Equations (A.1) to (A.4) and solving the equation system, the following final expressions can be derived for the atrazine, hydrogen peroxide and ferrous ion reaction rates, respectively:

$$R_{ATZ}(x,t) = -\frac{1}{\alpha}\left(k_2 C_{H_2O_2} C_{Fe^{2+}} + \Phi_{Fe^{2+},\lambda}\sum_{\lambda} e^{a}_{\lambda}(x,t)\right) \quad (A.12)$$

$$R_{H_2O_2}(x,t) = \left(-\frac{1}{\beta}\right) k_1 C_{H_2O_2} C_{Fe^{3+}} - \left(1 + \frac{\alpha'}{\alpha\beta}\right) k_2 C_{H_2O_2} C_{Fe^{2+}} - \left(\frac{\alpha'}{\alpha\beta}\right)\Phi_{Fe^{2+},\lambda}\sum_{\lambda} e^{a}_{\lambda}(x,t) \quad (A.13)$$

$$R_{Fe^{2+}}(x,t) = \Phi_{Fe^{2+},\lambda}\sum_{\lambda} e^{a}_{\lambda}(x,t)\left(\frac{1}{\alpha}\right)\left(\frac{2\alpha'}{\beta} + 1\right) + k_1 C_{Fe^{3+}} C_{H_2O_2}\left(\frac{2}{\beta}\right) + k_2 C_{Fe^{2+}} C_{H_2O_2}\left(\frac{1}{\alpha}\right)\left(\frac{2\alpha'}{\beta} - 2\alpha + 1\right) \quad (A.14)$$